Peripheral Milling of Wooden Materials without Cutter-Marks – A Mechatronic Approach

KLAUS RÖBENACK*, DANISH AHMED*,
STEPHAN ECKHARDT*, CHRISTIAN GOTTLÖBER**
* Technische Universität Dresden, Institute of Control Theory, 01062 Dresden, Germany
Email: klaus.roebenack@tu-dresden.de, danish.ahmed@tu-dresden.de, stephan.eckhardt@tu-dresden.de
** Technische Universität Dresden, Institute of Wood and Paper Technology, 01062 Dresden, Germany
Email: Christian.gottloeber@tu-drseden.de

Abstract: - Peripheral milling is an important cutting procedure to shape work pieces of wood. Because of the kinematical principle there are so-called cutter-marks on the surface of the work pieces after cutting which influence the quality. These surface patterns cannot be avoided completely and most of the time there are some efforts to smooth the surface by sanding or linear cutting afterwards which cost extra time and money. To improve this situation a new mechatronic approach is introduced to eliminate the cycloid motion track when the cutting edge approaches the work piece. In this way, the effective motion of the cutting edge is changed to a linear motion by means of piezo actuators or magnetic bearings.

Key-Words: - Peripheral milling, cutter-marks, surface quality, wood and wood based materials, active magnetic bearings, flatness-based control.

1 Introduction

Peripheral milling and sawing are two widely used cutting operations utilized to shape wooden work pieces [1, 2]. This process consists of a rotary cutting motion and a linear feeding motion. The combination of these two motions leads to a cutting-edge trajectory of a prolonged cycloid (Fig. 1). This trajectory creates a wavy structure on the work piece surface and that are called cutter-marks. Depending on the machining parameters, machine vibrations and tool accuracy these patterns are visible as small shadow stripes perpendicularly to the feeding direction of the work piece. This is caused by the periodic changing of the light reflection direction on the wavy surface.

Due to the principle of the milling procedure this structure is given and cannot be avoided completely. Mostly some smoothing operations like sanding or linear cutting are to be applied afterwards in the process chain to improve the surface quality. But that means extra efforts and process time, which translate to extra costs.

The regular cutter-mark is defined by its length, which is equal to the feed per tooth f_z [3], and its wave depth t_m. Both are connected by (1) with respect to the tool diameter *d*. Taking into account that the feed per tooth f_z depends on the feed speed v_f, the tool rotation number *n* and the tool edge number *z,* there are some possibilities to influence the appearance of the cutter-marks easily. If the tool has more than one cutting edge, all edges must have the same distance to the tool rotation axis. This is a ambitious task for tool manufacturers and the maintenance staff. Otherwise the wavy structure is mostly generated by only one cutting edge – the one with the biggest distance to the tool rotation axis.

$$t_m \approx \frac{f_z^2}{4 \cdot d} \tag{1}$$

$$f_z = \frac{v_f}{n \cdot z} \tag{2}$$

Currently the only way to minimize the introduced surface patterns is to adjust the machine carefully and to use precise tools. It is known that cutter-marks are nearly invisible when the feed per tooth f_z does not exceed a measure of 0.2 mm (tool diameter range up to 35 mm) or 1.5 mm (tool diameter range bigger than 100 mm). Also when touching the machined surface cutter-marks can be felt if the wave depth t_m exceeds 10 µm.

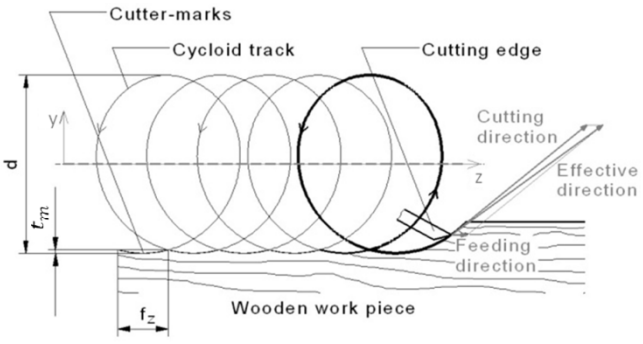

Fig. 1. Cutting edge trajectory and development of cutter-marks of peripheral milling (Climb cutting)

All in all the kinematics of peripheral milling and the accuracy demands limit the surface quality on the work piece. If one needs a surface quality without visible disturbances then one has to lower the feed speed v_f or increase the spindle rotation number n and the tool edge number z as well as the tool diameter d (following from (1) and (2)). There is always a compromise between high performance cutting and acceptable work piece quality when peripheral milling is performed. If one lowers the feed speed the quality improves but on the other hand processing time increases together with the production costs. That is why new methods must be found to avoid cutter-marks without necessarily influencing the factors mentioned above.

2 Approach

A way to solve the problem explained in the introduction is by employing actuator controlled motion of the tool spindle position to obtain a linear cutting motion when the cutting edge is in contact with the work piece (Fig. 2). That means the machine spindle position should be moved periodically in one dimension (y-direction according to Fig. 2) to generate a linear motion parallel to the work piece surface.

Therefore a new positioning mechanism on the tool spindle bearings must be applied to reduce or eliminate cutter-marks. In this context magnetic bearings or piezo-electric actuators can be used together with a specific control strategy.

The idea to control the tool edge position during the rotation is not new. Fischer and Rehm applied for a petty patent for a method for cutting of wooden or plastic work pieces [4], in which a radial moveable cutting edge within a milling tool is controlled by a cam mechanism. This system depends on a precise dynamical optimisation to avoid self destruction [5].

Besides the movement of only the edge within the tool a movement of the complete tool seems to be more realistic. There is some previous research work

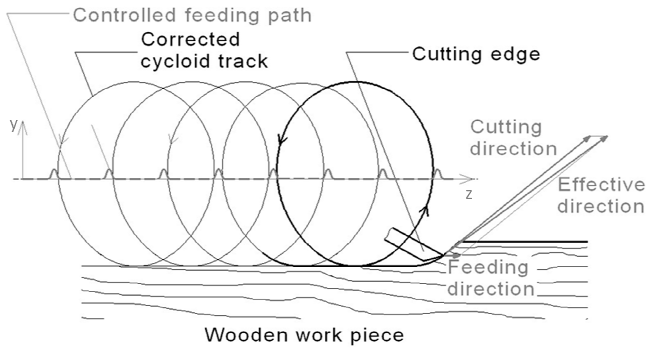

Fig. 2. Cutting edge trajectory and controlled y-z feeding path (dashed line) to avoid the development of cutter-marks in opposite to Fig. 1.

about non-circular drilling and circular machining at Technische Universität Dresden in co-operation with industrial partners [6, 7]. In this case magnetic bearings were used successfully.

The authors showed in [8] that a significant reduction in cutter-marks is possible using active magnetic bearings. Certain issues with system lag and overshoot will be address in this paper and a tuning strategy also presented.

The application of piezo-electric actuators to influence and control the spindle position when milling of wood was also shown and practical tested by Hynak et al. [9, 10] and Jackson et al. [11].

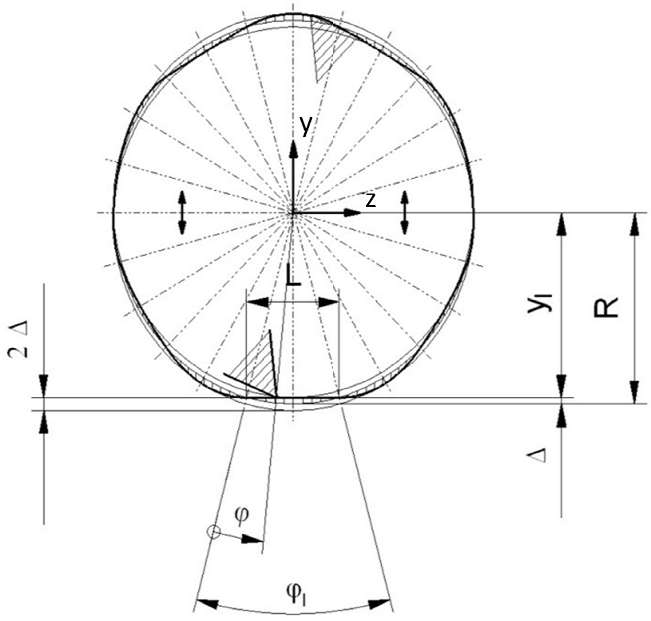

Fig. 3. Visualisation of the periodic vertical cutting edge motion depending on the rotation angle φ of the tool to generate the linear movement with length L.

The dimensions of the small periodic displacements of the tool perpendicularly to the feeding direction are only a few microns. This shall be realised with high frequency by the available electromechanical actuators or bearings. These actuators can be placed directly at the tool interface, that is, close to the spindle ball bearings.

The actuators set the tool to periodic oscillation in the y-direction synchronised to the rotational position of the cutting edge (Fig. 3). The period of tool axis oscillation is $2\varphi_l$, which is the double of the linearized rotation sector. It is possible to determine the amplitude Δ by using (3), which depends on the tool radius R and the linearized rotation sector φ_l. The frequency of oscillation must be an integer multiple of the tool rotation number.

$$\Delta = R - y_l = R \cdot \left[1 - \cos\left(\frac{\varphi_l}{2} \right) \right] \qquad (3)$$

The equations given below describe the two half periods of actuation in the y-direction. The desired vertical trajectory is a function of the rotation angle φ and depend on the linearized rotation sector φ_l and tool diameter R.

For $0° \le \varphi < \varphi_l$:

$$y(\varphi) = R \cdot \left[\cos\left(\frac{\varphi_l}{2} - \varphi\right) - \cos\left(\frac{\varphi_l}{2}\right) \right] \qquad (4)$$

For $\varphi_l \le \varphi \le 2\,\varphi_l$:

$$y(\varphi) = -R \cdot \left[\cos\left(\frac{3 \cdot \varphi_l}{2} - \varphi\right) - \cos\left(\frac{\varphi_l}{2}\right) \right] \qquad (5)$$

The desired vertical trajectory, along with the velocity and acceleration can be seen in Fig. 4.

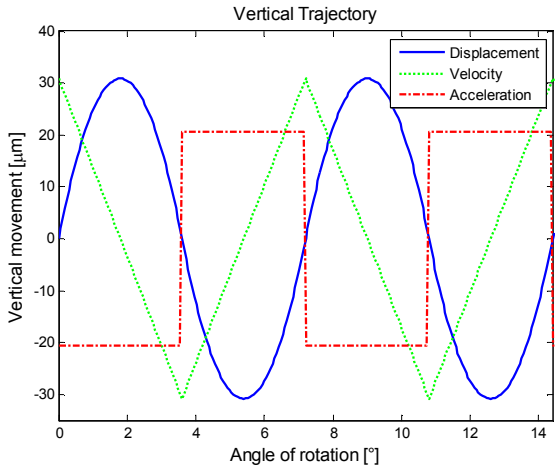

Figure 4. Desired trajectory of the spindle shown with (scaled) velocity and acceleration

The solution approach that is introduced and the following innovation improves the work piece quality and reduces the finishing activities after milling. The very high rotational speeds of wood milling tools may be lowered due to the changed process because of the possibility to reduce the cutter-marks. Tool wear is positively affected by the reduction in cutting speed. Also, cutting noise is lowered as the speed is reduced.

3 First Experiments

3.1 Design Preliminaries

The cutting tool is assumed to have two cutting edges. Therefore, the cutting edge is in contact with the work piece only when $0° < \varphi < \varphi_l$ and $180° < \varphi < 180° + \varphi_l$. So the trajectory of the cutting edges is theoretically not important during the non-cutting phase.

The cutting tool is required to have vertical displacement which is periodic in nature. This displacement depends on the tool diameter and the linearized rotation sector φ_l. The ratio between the revolution frequency and the vertical oscillation frequency is $N = 50$. In other words, for every revolution of the spindle, it oscillates 50 times in the vertical direction. Using this information, it is possible to calculate the linearized rotation sector angle

$$\varphi_l = \frac{360°}{2 \cdot N} = 3.6°.$$

Given a tool of diameter 125 mm, the radius $R = 62.5\ mm$, then the length L, shown in Fig. 3, can be estimated to be

$$L = 2 \cdot R \cdot \sin\left(\frac{\varphi_l}{2}\right) \approx 3.93 mm.$$

Using (3), the amplitude Δ can be obtained:

$$\Delta = 30.84 \mu m.$$

The amplitude Δ represents only half the total vertical displacement of the tool. This is because the tool axis oscillations are symmetric for both half periods, as described in (4) and (5). Therefore, the experimental setup has to be designed (selecting the actuators, sensors, etc.) in such a manner to allow for a minimum vertical displacement of $2\Delta = 62\ \mu m$.

3.2 Experimental Setup and Controller Structure

As shown in Fig. 5 and Fig. 6, the spindle consists of a rotor which is levitated by three-phase electromagnetic radial bearings in the front and rear. Each of these bearings consist of three horseshoe magnets, spaced around the rotor at an angle of 120° to each other.

Although axial motion is not required for the current experiments, an axial control mechanism is put in place. This consists of a standard magnetic axial disc bearing. A laboratory spindle is shown in Fig. 6 which has a rotor of mass 10 kg and length 0.6 m.

It must be remembered that irrespective of the direction of the current only an attractive force exists between an electromagnet and a ferromagnetic material.

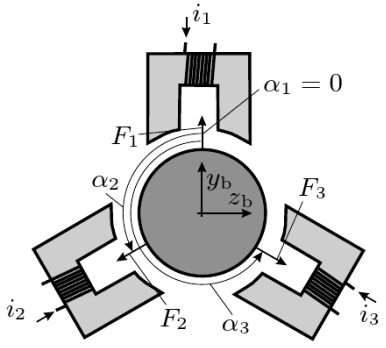

Figure 5: Radial bearing consisting of three horseshoe magnets

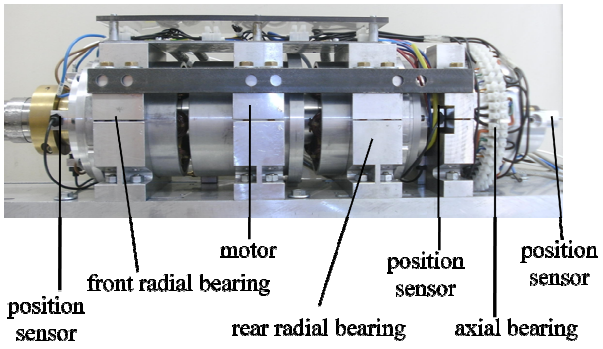

Figure 6: Laboratory spindle

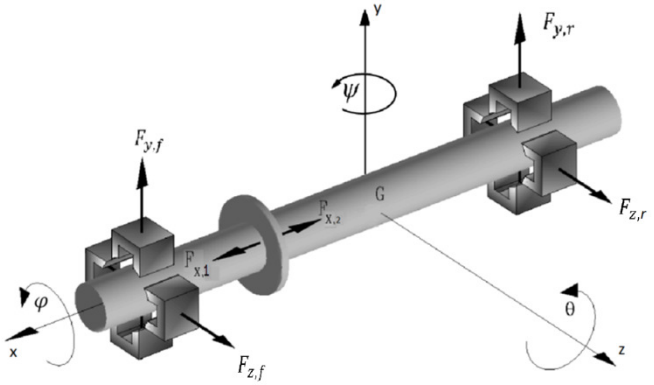

Figure 7: Magnetically levitated spindle

Therefore, eight independent controls are needed: One for each horseshoe magnet, totalling three per radial bearing and two for the axial bearing.

Switched transistor bridges are the power amplifiers used in the laboratory spindle. The eight independent currents can be controlled by varying the duty ratios of these transistor bridges. Current controlled amplifiers are widely used in industrial applications but in our setup current control is done by a cascaded controller, which is discussed in the next section. In our test-bench, the hardware used is dSpace 1103 [8].

3.3 Modeling

Modeling and controller design is described in [12, 13]. The mathematical modeling is done as follows: *x*, *y* and *z* are the cartesian coordinates of the centre of mass of the rotor in the axial, vertical and horizontal direction, respectively. Rigid-body motion is assumed. The spindle rotates about the *x*-axis and as long as the spindle does not rotate about the *y*- or *z*-axis, the axis of rotation, which is also the axis of symmetry, coincides with the *x*-axis. The angles ψ and θ describe the angular position of the rotor and φ is the angle of rotation. These angles are shown in Fig. 7.

The equations of motion of the rotor can be written as

$$
\begin{aligned}
m\ddot{x} &= F_x + mg_x \\
m\ddot{y} &= F_{y,f} + F_{y,r} + mg_y \\
m\ddot{z} &= F_{z,f} + F_{z,r} + mg_z \\
J_2\ddot{\psi} &= -(l_f - x)F_{z,f} + (l_r - x)F_{z,r} - J_1\dot{\phi}\dot{\theta} \\
J_2\ddot{\theta} &= (l_f - x)F_{y,f} - (l_r - x)F_{y,r} - J_1\dot{\phi}\dot{\psi} \\
J_1\ddot{\varphi} &= D_\varphi,
\end{aligned}
$$

where the distances from the centre of mass of the rotor to the front and rear bearing are given by l_f and l_r, respectively. The principal moments of inertia are given by J_1, J_2 and the mass of the rotor is denoted by m. F_x, F_y and F_z denote the forces in the *x*-, *y*- and *z*-direction, respectively. The indices *r* and *f* represent rear and front, respectively. The components of the gravitational acceleration are denoted by g_x, g_y and g_z. In case of appropriate adjustment we have $g_x = g_z = 0$ and $g_y = -g$, with $g = 9.81\ \mathrm{ms}^{-2}$.

All gyroscopic forces can be neglected and since the axial displacement is very small the model can be reduced to

$$
\begin{pmatrix} \ddot{y} \\ \ddot{z} \\ \ddot{\psi} \\ \ddot{\theta} \end{pmatrix} = M \cdot \begin{pmatrix} F_{y,f} \\ F_{z,f} \\ F_{y,r} \\ F_{z,f} \end{pmatrix} + \begin{pmatrix} -g \\ 0 \\ 0 \\ 0 \end{pmatrix} \qquad (6)
$$

with

$$
M = \begin{pmatrix} 1/m & 0 & 1/m & 0 \\ 0 & 1/m & 0 & 1/m \\ 0 & -l_f/J_2 & 0 & l_r/J_2 \\ l_f/J_2 & 0 & -l_r/J_2 & 0 \end{pmatrix}.
$$

The resultant force on each bearing is the sum of three independent forces, each one created by one horseshoe magnet. This can be seen in Fig. 5.

$$
\begin{pmatrix} F_{y,j} \\ F_{z,j} \end{pmatrix} = \begin{pmatrix} \sin(\alpha_1) & \sin(\alpha_2) & \sin(\alpha_3) \\ \cos(\alpha_1) & \cos(\alpha_2) & \cos(\alpha_3) \end{pmatrix} \begin{pmatrix} F_{1,j} \\ F_{2,j} \\ F_{3,j} \end{pmatrix},
$$

where $\alpha_1 = 0°$, $\alpha_2 = 120°$, $\alpha_3 = 240°$ and $j \in \{f, r\}$, and the forces generated by the horseshoe magnets are $F_{1,j}$, $F_{2,j}$ and $F_{3,j}$.

By neglecting the interaction of currents in different coils, saturation and other nonlinear effects, a simple force-current relationship is obtained [7]

$$
F_{k,j} = \mu_{k,j} \frac{i_{k,j}^2}{\left(s_j - y_j \sin\alpha_k - z_j \cos\alpha_k\right)^2}, \qquad (7)
$$

where *s* is the nominal air gap, $k \in \{1,2,3\}$, μ is a constant which depends on the bearing geometry and material, and *i* is the current.

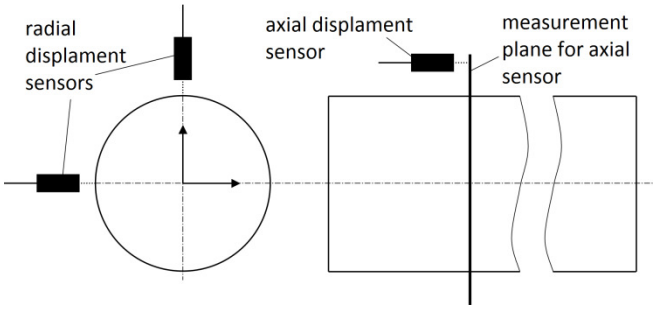

Figure 8. Contact free sensors used to measure radial and axial displacement

If the desired force $F_{k,j}$ is known, the relationship given above can be used to calculate the required current inputs. These inputs serve as the controls of a flatness-based position tracking controller.

The modelling of the coil current in each independent horseshoe magnet is done as follows [6]:

$$\frac{d}{dt}(Li) = u - Ri,$$

where i is the current, R is the resistance of the coil, u is the input voltage and L is the inductance which depends on the rotor position.

A contact-free incremental sensor is used to measure the rotor angular position about the x-axis. This measurement, i.e. the angle of rotation of the rotor, is needed to synchronize the tool path with rotor rotation. As shown in Fig. 8, the orientation and position of the rotor is measured with two pairs of eddy current sensors in two planes perpendicular to the axis of symmetry. One more eddy current sensor is used to measure the axial rotor position. For trajectory tracking the rotor position and orientation is required.

3.4 Controller Design

A system has the flatness property if it is possible to select or choose a set of outputs such that all the states and inputs of the system can be expressed explicitly as a function of the flat outputs and their (finite number of) time derivatives. A system which has this property is called flat. Except for control/input-affine nonlinear systems [14], there is no general systematic method of finding flat outputs for nonlinear systems [15]. Therefore, it is not always possible to know if a system is flat or not. Nevertheless, if flat outputs are found, then the concept of flatness can be easily used to extend the notion of controllability from linear to non-linear systems. In particular, flatness-based control is extremely useful for trajectory tracking.

The general nonlinear system

$$\boldsymbol{F}\left(\boldsymbol{z}, \dot{\boldsymbol{z}}, \dots, \boldsymbol{z}^{(\alpha)}\right) = \boldsymbol{0},$$

with the system variables $\boldsymbol{z} = (z_1, \dots, z_s)$ is flat if there exists a vector $\boldsymbol{y} = (y_1, \dots, y_m)$ which is a function of the system variables and its derivatives such that the following conditions are fulfilled:

1. The components of $\boldsymbol{y}$ are differentially independent, that is, they do not satisfy any non-trivial differential equation of the form given below:

$$\boldsymbol{R}\left(\boldsymbol{y}, \dot{\boldsymbol{y}}, \dots, \boldsymbol{y}^{(\delta)}\right) = \boldsymbol{0}.$$

2. The system variables $\boldsymbol{z}$ can be represented as a function of $\boldsymbol{y}$ and a finite number of its time derivatives.

Each vector $\boldsymbol{y}$ is called a flat output of the system if it fulfils the above conditions [15].

Consider the nonlinear state-space system with the states $\boldsymbol{x}$ and input $\boldsymbol{u}$ [16]:

$$\dot{\boldsymbol{x}}(t) = \boldsymbol{f}\left(\boldsymbol{x}(t), \boldsymbol{u}(t)\right), \tag{8}$$

where $\boldsymbol{x}(t) \in R^n$, $\boldsymbol{u}(t) \in R^m$, $m \leq n$ and

$$rank\left(\frac{\partial \boldsymbol{f}(\boldsymbol{x}, \boldsymbol{u})}{\partial \boldsymbol{u}}\right) = m \tag{9}$$

in some open and dense subset. This condition means that there are m independent control inputs.

The nonlinear system is flat if it is possible to choose m number of independent (possibly fictitious) outputs, denoted by $\boldsymbol{y}$, and finite multi-integers l and r, such that

$$\boldsymbol{y} = (y_1, y_2, \dots, y_m) = \boldsymbol{g}\left(\boldsymbol{x}, \boldsymbol{u}, \dot{\boldsymbol{u}} \dots, \boldsymbol{u}^{(l)}\right). \tag{10}$$

The states and inputs can then be expressed as a function of the output and a finite number of its time derivatives, as can be seen from (11) and (12). It should be noted that $\boldsymbol{u}$ and $\boldsymbol{y}$ have the same number of components, that is, the number inputs is equal to the number of outputs. Then $\boldsymbol{x}$ and $\boldsymbol{u}$ can be represented as

$$\boldsymbol{x} = \boldsymbol{h}_1\left(\boldsymbol{y}, \dot{\boldsymbol{y}}, \dots, \boldsymbol{y}^{(r)}\right), \tag{11}$$

$$\boldsymbol{u} = \boldsymbol{h}_2\left(\boldsymbol{y}, \dot{\boldsymbol{y}}, \dots, \boldsymbol{y}^{(r+1)}\right), \tag{12}$$

where

$$\boldsymbol{u}^{(l)} = \left(u_1^{(l_1)}, \dots, u_m^{(l_m)}\right)$$

and

$$\boldsymbol{y}^{(r)} = \left(y_1^{(r_1)}, \dots, y_m^{(r_m)}\right).$$

A linear system is flat if and only if it is controllable. It should be noted that integration is not required for flatness-based trajectory planning.

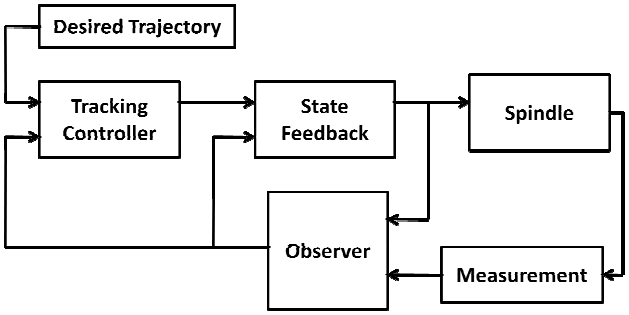

Figure 9. Signal flow diagram of the feedback control system.

For the controller design [17] the rigid body model is used (6). This controller has a cascade structure. The reference currents are calculated by the outer loop, that is the position or tracking controller, shown in Fig. 9. The inner controller is used to follow these reference currents.

3.5 Tracking Control

The position and orientation of the rotor are selected as flat outputs for the problem at hand, that is

$$\boldsymbol{y} = (y, z, \psi, \theta)^T .$$

If the tracking error in the vertical direction is defined as $e_y := y^{ref} - y$, imposing the error dynamics:

$$\left(\frac{d}{dt} + \lambda_{y,1}\right)\left(\frac{d}{dt} + \lambda_{y,2}\right) e_y = 0,$$

the following is obtained:

$$\ddot{e}_y = \left(\lambda_{y,1} + \lambda_{y,2)}\right)\dot{e}_y - \lambda_{y,1}\lambda_{y,1} e_y. \qquad (13)$$

Since $\ddot{e}_y = \ddot{y}^{ref} - \ddot{y}$, the resulting equation for the acceleration in the vertical direction is

$$\ddot{y} = \ddot{y}^{ref} + \left(\lambda_{y,1} + \lambda_{y,2)}\right)\left(\dot{y} - \dot{y}^{ref}\right) - \lambda_{y,1}\lambda_{y,2}\left(y - y^{ref}\right).$$

If the eigenvalues of the dynamics of the tracking error $\lambda_{y,1}$ and $\lambda_{y,2}$ are chosen so they are symmetric about the real axis and in the open left side of the complex plane, a stable system is attained.

For the controller design of the whole system we introduce the auxiliary variables a_y, a_z, a_ψ, a_θ as follows:

$$\begin{pmatrix} a_y \\ a_z \\ a_\psi \\ a_\theta \end{pmatrix} = \begin{pmatrix} \ddot{y} \\ \ddot{z} \\ \ddot{\psi} \\ \ddot{\theta} \end{pmatrix}.$$

A stable controller is required for each one of the uncoupled systems. The reference or desired trajectory coordinates are denoted by y^{ref}, z^{ref}, ψ^{ref}, θ^{ref}.

The tracking error may be introduced as:

$$e = \begin{pmatrix} e_y \\ e_z \\ e_\psi \\ e_\theta \end{pmatrix} = \begin{pmatrix} y^{ref} \\ z^{ref} \\ \psi^{ref} \\ \theta^{ref} \end{pmatrix} - \begin{pmatrix} y \\ z \\ \psi \\ \theta \end{pmatrix},$$

where the position coordinates of the rotor are given by y and z and the orientation angles of the rotor given by ψ and θ. Imposing error dynamics for each coordinate as in (13), we obtain the error dynamics of the whole system as

$$\ddot{e} + K_1\dot{e} + K_0 e = 0, \qquad (14)$$

where K_0 and K_1 have real positive entries and are diagonal matrices. Then the auxiliary variables are given by

$$\begin{pmatrix} a_y \\ a_z \\ a_\psi \\ a_\theta \end{pmatrix} = \begin{pmatrix} \ddot{y} \\ \ddot{z} \\ \ddot{\psi} \\ \ddot{\theta} \end{pmatrix} = \begin{pmatrix} \ddot{y}^{ref} \\ \ddot{z}^{ref} \\ \ddot{\psi}^{ref} \\ \ddot{\theta}^{ref} \end{pmatrix} + K_1\dot{e} + K_0 e.$$

From the rigid body model the corresponding forces can be obtained (4):

$$\begin{pmatrix} F_{y,f} \\ F_{z,f} \\ F_{y,r} \\ F_{z,r} \end{pmatrix} = M^{-1} \cdot \left(\begin{pmatrix} a_y \\ a_z \\ a_\psi \\ a_\theta \end{pmatrix} - \begin{pmatrix} g_y \\ g_z \\ 0 \\ 0 \end{pmatrix} \right) \qquad (15)$$

or

$$\begin{pmatrix} F_{y,f} \\ F_{z,f} \\ F_{y,r} \\ F_{z,r} \end{pmatrix} = M^{-1} \cdot \begin{pmatrix} a_y + g \\ a_z \\ a_\psi \\ a_\theta \end{pmatrix}.$$

A nonlinear controller was implemented and this was an important part of the experimental setup. A flatness-based controller design methodology, as described in Section 3.4 was used. One may have to deal with complicated symbolic expressions during nonlinear controller design. Instead it is possible to use algorithmic or automatic differentiation [18, 19]. This approach was used successfully in [20], for nonlinear controller design for magnetic bearings.

3.6 Trajectory Planning

It may be assumed that the angular velocity $\dot{\varphi} = \omega$ of the rotor is constant, then $\ddot{\varphi} = 0$.

Since the desired trajectory is limited to movement in the vertical direction, the following trajectory equations are obtained:
Vertical movement:

$$y^{ref} = R\left[\cos\left(\frac{\varphi_l}{2} - \varphi\right) - \cos\left(\frac{\varphi_l}{2}\right)\right]$$

$$\dot{y}^{ref} = \omega R \cdot \sin\left(\frac{\varphi_l}{2} - \varphi\right)$$

$$\ddot{y}^{ref} = -\omega^2 R \cdot \cos\left(\frac{\varphi_l}{2} - \varphi\right).$$

Movement in the axial direction:

$$x^{ref} = \dot{x}^{ref} = \ddot{x}^{ref} = 0.$$

Movement in the horizontal direction:

$$z^{ref} = \dot{z}^{ref} = \ddot{z}^{ref} = 0.$$

Tilting of the spindle:

$$\psi^{ref} = \dot{\psi}^{ref} = \ddot{\psi}^{ref} = 0,$$
$$\theta^{ref} = \dot{\theta}^{ref} = \ddot{\theta}^{ref} = 0.$$

3.7 Calculating the Control Current

The required currents in each horseshoe magnet must be calculated. This may be done by using (9) to first calculate the net resultant desired force in each bearing. Due to the geometry and design of the radial bearings, there is no unique combination of currents that may be used to obtain the desired resultant force.

Hence, it is necessary to choose of force arbitrarily. Choosing

$$F_{1,j} = \begin{cases} F_{0,j} & if\ F_{y,j} \le -\dfrac{|F_{y,j}|}{\sqrt{3}} \\ F_{0,j} + F_{y,j} + \dfrac{|F_{z,j}|}{\sqrt{3}} & \text{otherwise,} \end{cases}$$

where $F_{0,j}$ is some arbitrarily chosen non-negative value and $j \in \{f, r\}$. The other forces can be calculated as follows:

$$F_{2,j} = F_{1,j} - F_{y,j} - \frac{F_{z,j}}{\sqrt{3}},$$

$$F_{3,j} = F_{1,j} - F_{y,j} + \frac{F_{z,j}}{\sqrt{3}}.$$

4 Experimental Results

As noted earlier, the rotor completes one vertical oscillation for every 7.2° change in the rotation angle. Therefore, for a rotational frequency of 100 rpm, the vertical oscillation frequency is 5000 rpm or about 523.6 rad/s or 83.3 Hz.

If the cutter-head has only two cutting egdes, then the cutting edge comes into contact with the work piece only for $0 \le \varphi \le \varphi_l$ and $180° \le \varphi \le 180° + \varphi_l$, where $\varphi_l = 3.6°$ and the cutting starts at $\varphi = 0$. This was taken into consideration when the controller parameters were fine-tuned.

Fig. 9 shows the desired vertical displacement required along with the actual vertical displacement achieved. An over-shoot is clearly observed along with a delay/phase-angle.

The desired trajectory of the cutting edge can be seen in Fig. 10. Had there been no vertical movement of the spindle the cutting edge would follow the circle, leading to the creation of cutter-marks. If the cutting edge follows the desired trajectory perfectly then a flat surface is produced, as shown by the horizontal dashed line. The actual path is also shown in Fig. 10. It can be seen that the delay and overshoot cause the cutting edge to deviate from the desired path; nevertheless, significant improvement is achieved, that is, the size of the cutter-marks is reduced.

It is obvious from Fig. 9 that there is a lag in the system. The actual trajectory seems to follow the desired trajectory with a lag which appears to be rather constant. One way to eliminate lag is to shift the reference trajectory so that it coincides with actual trajectory.

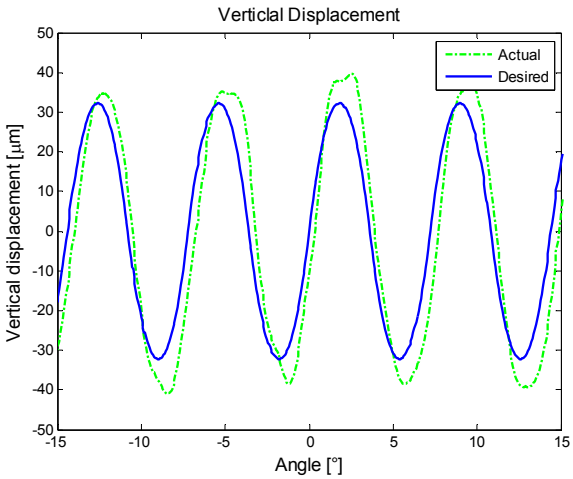

Figure 9: Plot of the desired and actual vertical displacement of the rotor

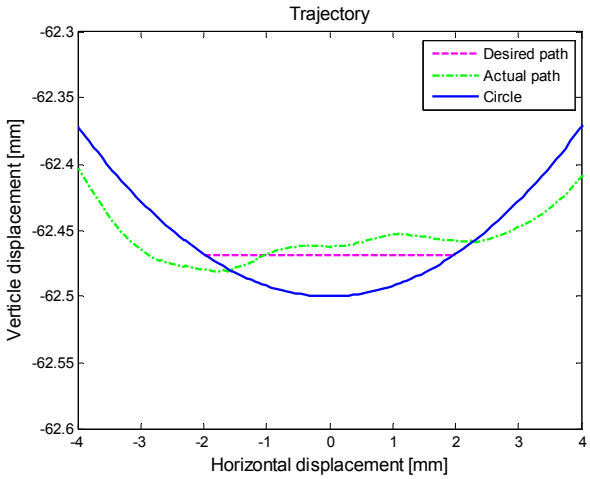

Figure 10: Trajectory of the cutting-edge (scaled)

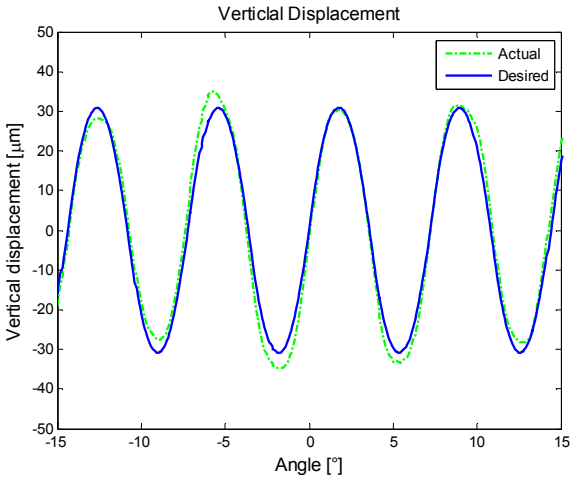

Figure 11: Plot of the desired and actual vertical displacement of the rotor

Define

$$\varphi_f = \varphi + k_1 T_a \omega$$

where k_1 is an integer, T_a is the sampling time and φ_f is the angle of rotation after k_1 number of time steps.

The lag can be eliminated by choosing an appropriate value for k_1. To achieve this goal, define

$$y_f^{ref} = R\left[\cos\left(\frac{\varphi_l}{2} - \varphi_f\right) - \cos\left(\frac{\varphi_l}{2}\right)\right],$$

where y_f^{ref} is the desired reference trajectory with respect to φ_f. This yields the reference acceleration:

$$\ddot{y}_f^{ref} = -\omega^2 R \cdot \cos\left(\frac{\varphi_l}{2} - \varphi_f\right).$$

Then a new reference trajectory is defined as follows:

$$y_{new}^{ref} = y^{ref} + k_2\left(y_f^{ref} - y^{ref}\right).$$

The new reference trajectory, y_{new}^{ref}, is a linear combination of the current reference trajectory and the reference trajectory k_1 number of time steps in the future. The use of this new reference trajectory helps eliminate the time lag.

Similarly, the new reference acceleration is defined as

$$\ddot{y}_{new}^{ref} = \ddot{y}^{ref} + k_3\left(\ddot{y}_f^{ref} - \ddot{y}^{ref}\right).$$

As opposed to the new reference trajectory, which helps eliminate lag, the new reference acceleration can be used to eliminate the overshoot that is apparent in Fig. 9, with the appropriate choice of the tuning parameter k_3.

It can be seen in Fig. 11 and Fig. 12 that significant improvement is achieved. There exists certain systematic noise in the system due to structural inhomogeneity (see Fig. 14). This can be observed by looking at the tracking error over a number of revolutions of the spindle. Therefore, it is important to adjust for k_2 and k_3 according to the angle during which the cutting will take place.

It can seen from Fig. 13 that the tracking error for the case with adjustment is much lower than the case without adjustment. Specifically, during the cutting phase $0° < \varphi < 3.6°$ the error is extremely small. The large error for the case without adjustment can be attributed to the lag and not the overshoot.

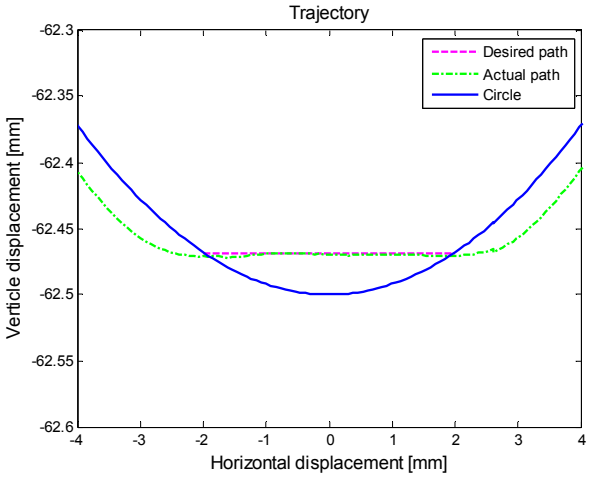

Figure 12: Plot trajectory of the cutting-edge (scaled)

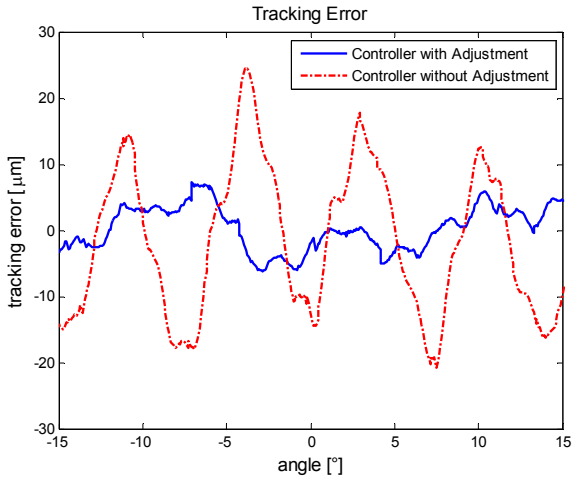

Figure 13: Tracking error

5 Conclusions and Outlook

Milling operation on wood produces specific surface patterns knows as cutter-marks. This is due to the kinematic relation between cutting tool and the work piece, and the exact shape of the cutter-marks are dependent on the cutting parameters such as the number of cutting edges, feed speed, etc. The method used to reduce or eliminate cutter-marks is by periodic actuation of the cutting tool in order to produce linear motion during the cutting phase. The vertical motion of the cutting tool is in the micron-range.

The authors had shown in [8] that active magnetic bearings can be used to reduce cutter-mark depth. Improvements were suggested and implemented in this study and the results show significant improvement in the reduction of the grooves formed. In particular, both the overshoot and the delay have been eliminated for all practical purposes.

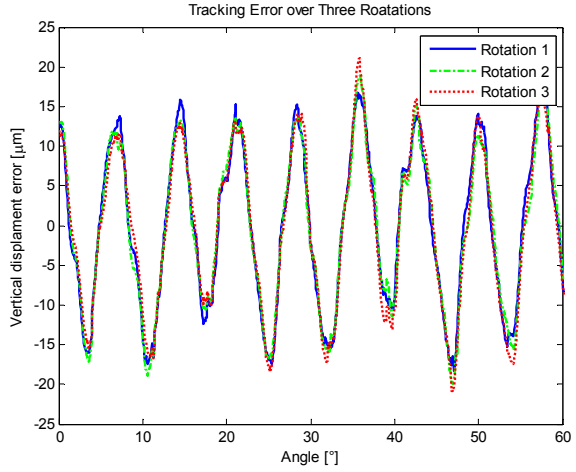

Figure 14: Tracking error plotted over three revolutions

In future works, the reference trajectory may be changed to reduce or eliminate the vertical oscillations during the non-cutting phase. In addition, a reference trajectory can be chosen so that the required acceleration is not discontinuous. Furthermore, Fourier analysis will be used to derive a systematic method for a further reduction of the tracking error. The results will be presented in upcoming publications.

Acknowledgement

The authors would like to thank Dipl.-Ing. Christian John for his help and support.

References:

[1] A. Wagenführ and F. Scholz (Ed.), *Taschenbuch der Holztechnik* (Fachbuchverlag, Leipzig, Germany, 2012).

[2] G. Maier, *Holzspanungslehre* (Vogel Buchverlag, Würzburg, Germany, 2000).

[3] DIN 6580, *Begriffe der Zerspantechnik; Bewegungen und Geometrie des Zerspan-vorganges*, 1985.

[4] R. Fischer and K. Rehm, *Einrichtung zur spanenden Bearbeitung von Werkstücken aus Holz, Kunststoffen oder dgl.*, Petty Patent 195 17 596.4, 13.05.1995.

[5] R. Fischer and C. Gottlöber, *Verbesserung der Oberflächenbearbeitung von Holz mit geometrisch bestimmten Schneiden durch lineare Schnitt-bewegung*, AiF Final Report, AiF-Project 10811 B/1, 1998.

[6] J. von Löwis, J. Rudolph, J. Thiele, F. Urban, Flatness-based Trajectory Tracking Control of A Rotating Shaft, *Proc. Seventh International Symposium on Magnetic Bearings*, ETH Zurich, Switzerland, pp. 299-304, 2000.

[7] J. Thiele, F. Urban, J. von Löwis, J. Rudolph, Neue Anwendungen für magnetgelagerte Spindeln, *Werkstatt und Betrieb*, vol. 134, no. 7/8, pp. 127-129, 2001.

[8] C. Gottlöber, K. Röbenack, D. Ahmed and S. Eckhardt, An Approach for Actuator Controlled Motion of Peripheral Milling Tools on Wood. *International Journal of Engineering Research and Applications (IJERA)*, vol. 2, issue 6, pp. 1208-1213, 2012.

[9] P. Hynek, *Wood Surface Form Improvement by Real Time Displacement of Tool Trajectory*, doctoral diss., Loughborough University, Great Britain, 2004.

[10] P. Hynek, M.R. Jackson, R. Parkin, N. Brown, Improving wood surface form by modification of the rotary machining process, *Proc. of the Institution of Mechanical Engineers, Part B: Journal of Engineering Manufacture*, vol. 218, no. 8, pp. 875-887, 2004.

[11] M.R. Jackson, P. Hynek, R.M. Parkin, Active Timber machining: From Theory to Reality, *Proc. 50. Internationalen Wissenschaftlichen Kolloquiums*, TU Ilmenau, Germany, 2005.

[12] S. Eckhardt and J. Rudolph, High Precision Synchronous Tool Path Tracking with an AMB Machine Tool Spindle, in *Ninth International Symposium on Magnetic Bearings*, Lexington Kentucky, USA, 3-6 August, 2004.

[13] J. Rudolph, F. Woittennek, and J. v. Löwis, *Zur Regelung eine elektromagnetische gelagerten Spindel*. at - Automatisierungstechnik, vol. 48, no. 3, pp. 132-139, 2000.

[14] M. Franke, K. Röbenack, Some remarks concerning differential flatness and tangent systems. Proc. in Applied Mathematics and Mechanics (PAMM), vol. 12, no. 1, pp. 729-730, 2012.

[15] K. Schlacher, M. Schöberl: Construction of flat outputs by reduction and elimination. Proc. 7th NOLCOS, pp. 666-671, 2007.

[16] P. Rouchon, M. Fliess, J. Levine, and P. Martin, Flatness and defect of nonlinear systems: Introductory theory and examples*, International Journal of Control*, vol. 61, no. 6, pp. 1327–1361, 1995.

[17] J. Levin, J. Lottin, and J. C. Ponsart, A nonlinear approach to the control of magnetic bearings. *IEEE Trans. Control Systems Technology*, vol 4, no. 5, pp. 524-544, 1996.

[18] K. Röbenack and K. J. Reinschke, Reglerentwurf mit Hilfe des Automatischen Differenzierens *at - Automatisierungstechnik,* vol. 48, no. 2, pp. 60-66, 2000.

[19] K. Röbenack, Automatic Differentiation and Nonlinear Controller Design by Exact Linearization. *Future Generation Computer Systems*, vol. 21, no. 8, pp. 1372-1379, 2005.

[20] S. Palis, M. Stamann, and T. Schallschmidt, Nonlinear control design for magnetic bearings via automatic differentiation, *in Proc. 13th Power Electronics and Motion Control Conference*, pp. 1660 - 1664, 2008.